공학석사학위논문

수직축 풍력발전기 주위 유동에 대한 실험적 연구 및 돌기를 이용한 유동 제어

Experimental study on the flow around a vertical axis wind turbine and its control using tubercles

2019 년 2 월

서울대학교 대학원

기계항공공학부

김 종 현

수직축 풍력 발전기 주위 유동에 대한 실험적 연구 및 돌기를 이용한 유동 제어

Experimental study on the flow around a vertical axis wind turbine and its control using tubercles

지도교수 최 해 천

이 논문을 공학석사 학위논문으로 제출함

2018 년 10 월

서울대학교 대학원

기계항공공학부

김 종 현

김종현의 공학석사 학위논문을 인준함

2018 년 12 월

위 원 장 송 성 진

부위원장 최 해 천

위 원 김 효 영

Experimental study on the flow around a vertical axis wind turbine and its control using tubercles

Jonghyun Kim
Department of Mechanical & Aerospace Engineering
Seoul National University

Abstract

In the present study, an experimental study was conducted to investigate the unsteady flow characteristics of the flow around the vertical axis wind turbine and to improve the aerodynamic performance of the vertical axis wind turbine by using tubercles. The experiments were conducted at operating condition where $Re = 1.2 \times 10^5$ based on rotor diameter and rotating speed was 300 1100 rpm. The performance factor, the power coefficient which indicates a measure of the relative kinetic energy extracted from the flow, was measured by a rotary torque transducer and the velocity field was obtained by using a phase-averaged particle image velocimetry. As the rotor rotates, the dynamic stall occurs at the blade leading edge of the suction surface. We suggested the tubercles to control dynamic stall. By using tubercles to leading edge of the suction surface, the stall delayed, which improve the aerodynamic performance of the rotor.

Keywords: vertical axis wind turbine, bio-mimetic flow control, leading-edge

tubercles, streamwise vortices, dynamic stall delay

Student number: 2016-20649

Contents

List of Figures

Figure

Nomenclature

Roman Symbols

A	planform area of the model
c	chord length
R	rotor radius
D	rotor diameter
H	rotor height
N	number of blades
U	free-stream velocity
U_{rel}	relative velocity
d	tubercle diameter
s	tubercle spacing
$\bar{T}$	averaged torque in experiment
$\bar{P}$	averaged power in experiment
$\bar{C_p}$	averaged power coefficient
Re_D	Reynolds number based on the rotor diameter
x, y, z	cartesian coordinate with the origin at the center of the model
x', y', z'	cartesian coordinate with the origin at the center of the blade

Greek Symbols

α	angle of attack
θ	azimuthal angle
ν	kinematic viscosity

ρ	density of air
λ	tip-speed-ratio
λ_{opt}	optimum tip-speed-ratio
ω	rotational velocity
ω_y	streamwise vorticity
$\omega_{z'}$	z'-directional vorticity

Abbreviations

PIV	particle image velocimetry
FoV	field of view

Chapter 1

Introduction

Wind energy has been one of the leading renewable energy sources to reduce dependence on fossil fuel. Most of this energy is produced using large scale horizontal axis wind turbines (HAWTs) which can generate over 4 MW individually with bade diameters up to 126 m as shown in Figure 1.1 (Vestas, 2018). HAWTs are very efficient when operating individually, extracting nearly the theoretical Betz limit of 59% of the power of the wind (Vanek & Albright, 2008). However, HAWTs evolve a relatively large wake, so there is a limitation to construct wind farm with HAWTs. Due to aerodynamic interference between adjacent HAWTs, turbines are typically spaced 3 to 5 rotor diameters in the streamwise direction to obtain about 90% of the power output of an isolated HAWTs (Hau, 2013). Small scale vertical axis wind turbine (VAWTs) represent an alternative to HAWTs with fewer restrictions on their spacing to construct wind farm. VAWTs have advantages of insensitivity to wind direction, which is capable of generating power without yawing into the wind direction, relatively quiet operating condition due to slower blade rotation and a typically simple design, resulting in low construction and maintenance cost due to fewer moving parts and a constant blade profile along the span (Islam *et al.*, 2007; Howell *et al.*, 2010; Greenblatt *et al.*, 2013). Wittlesey *et al.* (2010) developed a wind farm model based on the fluid dynamics of fish schooling, indicating a potential increase in power density defined as power produced per unit area due to the

decreased turbine spacing. Dabiri *et al.* (2011) tested this idea, using arrays of VAWTs and claimed that a wind farm using VAWTs can have more power density than that of HAWTs because VAWTs have less aerodynamic interference so can be placed close to each other relatively. The representative flow characteristic of VAWTs is known as dynamic stall. The dynamic stall occurs when an airfoil undergoes unsteady motions at higher angles of attack than stall angle of a steady airfoil. The kinematics of the blades of the VAWT is shown in Figure 1.2. The blades of the VAWT experience negative and positive angle of attack continuously by a rotation as shown in Figure 1.3. Since the blades of the VAWT operating in unsteady flow overcome the static stall angle, the dynamic stall occurs (Leishmanl, 2002). During dynamic stall, large leading edge separated vortices are formed and then they shed from the airfoil, resulting in a performance decreases (Ferreira *et al.*, 2009). Many studies found that dynamic stall occurs around the blades of VAWTs by using experimental studies (Fujisawa & Shibuya, 2001; Ferreira *et al.*, 2009; Edwards *et al.*, 2015) or using numerical simulations (Tsai & Colonius, 2016; Posa *et al.*, 2016), and claimed that aerodynamic performance on VAWT can be increased by delaying the stall (Roh & Kang, 2013; Elkhoury *et al.*, 2015). Meanwhile, in flow control studies, many researchers developed ideas to control the unsteady flow. Especially, leading edge modification is well known for controlling unsteady flows in many engineering applications. Miklosovic *et al.* (2004) investigated the effect of leading edge tubercles, which achieved separation delay of stalled airfoil. Narayanan *et al* (2015) showed that the leading edge serration is effective even on airfoils of low angle of attack. Also, Kim *et al* (2018) obtained increased aerodynamic performance by using leading edge tubercles. The leading edge tubercles or serrations induce streamwise vortices which control the unsteady flow downstream. These methods could be applied to the VAWT blades for controlling

the unsteady flow characteristics. In present study, the flow around a VAWT is investigated by using particle image velocimetry and aerodynamic performance is measured by using torque measurement. After the flow investigation, tubercles are applied to the blades of a VAWT that result in enhancement of the aerodynamic performance and the flow fields of the VAWT with and without tubercles are compared.

Figure 1.1. A pictures of a large scale horizontal axis wind turbine (HAWT) and a small scale vertical axis wind turbine (VAWT).

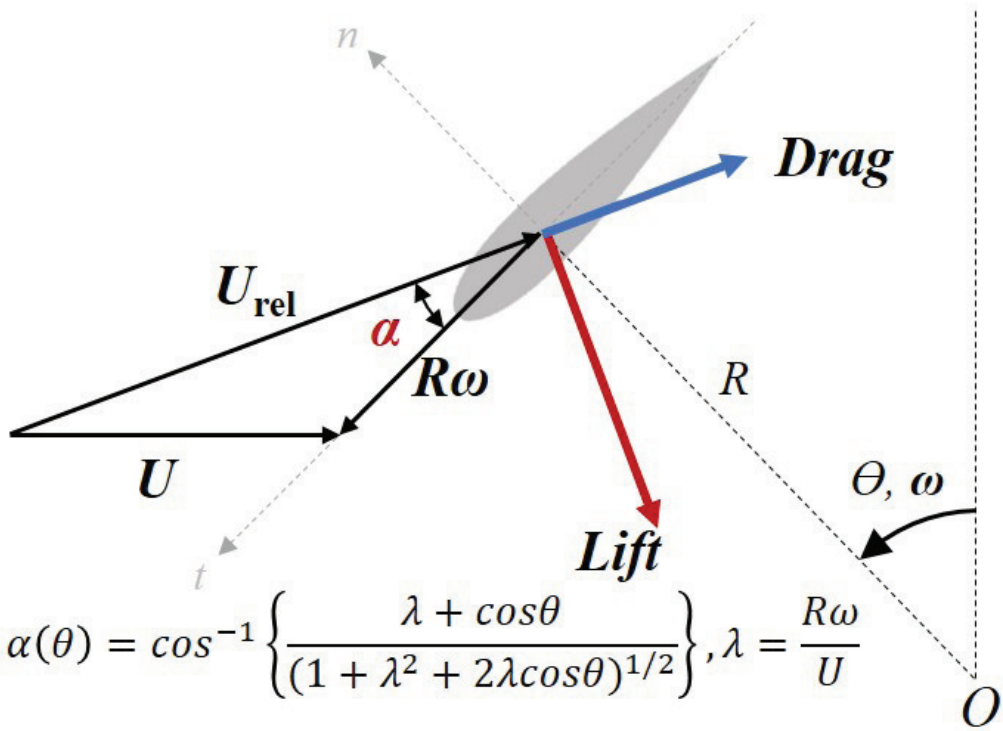

Figure 1.2. The kinematics of the blades of a VAWT.

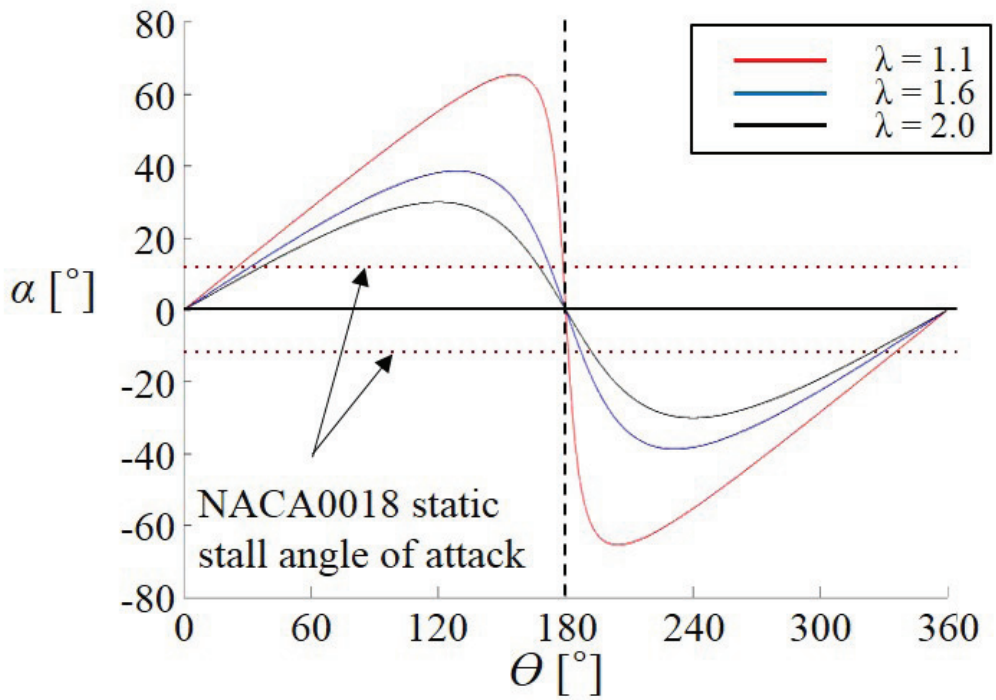

Figure 1.3. The angles of attack variation over typical VAWT blade, for = 1.1, 1.6 and 2.0. Compared to static stall angle of attack of NACA0018 at Re = 80,000.

Chapter 2

Experimental Set-up

2.1 VAWT model geometry

We construct a VAWT model by using three-dimensional surface data as shown in Figure 2.1. The model shape except for the blades is composed of three-dimensional surface data of commercial VAWT Aeolos-V 300W (Aeolos, 2018), where the scale of the model was set to 1:3. The blade consisted of a NACA0018 airfoil with 0.9 m chord extruded to a length of 0.4 m. The rotor had a diameter of 0.3 m, as measured by a circle tangent to the chord of each airfoil.

2.2 Parameters of tubercles

To control the unsteady flows, we introduced the leading edge tubercles. Two parameters are chosen to investigate the effect of tubercles. As shown in Figure 2.2, diameter (d) of tubercles and spacing (s) between tubercles are the parameters that determine the tubercles. For convenience, tubercles made of hemispherical styrofoam are attached uniformly from the leading edge of the airfoil on the suction side.

2.3 Torque measurements

Experiments were conducted in a closed-type wind tunnel (Gttingen type), whose test section is 0.9 m wide, 0.9 m high and 4 m long. The maximum wind speed in the test section is 60 m/s and the uniformities of the mean streamwise velocity and the turbulence intensity are both within 0.3% at the free-stream velocity of 20 m/s. In all experiment, the freestream velocity was 6 m/s, i.e. a Reynolds number based on the rotor diameter ($Re_D = UD/\nu$) was 1.2×10^5, where D is the rotor diameter and ν is the kinematic viscosity of air. The rotor was mounted to shafts in both directions, as depicted in Figure 2.3. The height of the shaft was adjusted to locate the rotor at the center of the wind tunnel. The VAWT model is rotated by BLDC motor (TM13-A2053 TM TECH-i). And the model shaft was connected to a rotary torque transducer (T22/5NM, HBM) between the rotor and the BLDC motor. The torque transducer present a difference between a motor supplying and lift driven, then the positive sign means the aerodynamic force driven torque surplus motor driven. The torque transducer had a 0-5 Nm^{-1} measurement range with a maximum system error of +0.020% rated output (i.e. + 0.001 Nm^{-1}) in clockwise and counterclockwise torque. An optically clear, cast acrylic sheet was suspended to be flush with the free surface in order to eliminate surface distortion. The shaft is connected to a ball and thrust bearing which located upper and under the test section, minimizing a friction loss. Also, the VAWT blade is located in the center of the test section.

2.4 Particle image velocimetry

In the VAWT, the flow characteristics are continuously changed depending on the position of the blades due to the blowing flow, so that the aerodynamic

performance acting on the blades also changes depending on the position of the blades. So, it is essential to measure the flow field depending on the blade position. To obtain the flow characteristics depending on the blade position, the phase-averaged particle image velocimetry (phase-averaged PIV) was conducted as shown in Figure 2.4. Since we mainly focus on the flow near the blade, we synchronized the instantaneous velocity fields by a laser tachometer. Figure 2.3 shows the experimental setup for phase-averaged PIV. We performed PIV in two XZ planes with tip-speed-ratio (TSR, $\lambda = R\omega/U$) changes. PIV measurements were conducted at λ=1.1 and $\theta = 60^\circ$ to 90° as increment 10°, and $\theta = 120^\circ$, respectively. The experiment is held at the operating point where the rotational speed is 300 - 1100 rpm, respectively. The laser used for illumination is a Nd:Yag laser having maximum repetition is 15Hz, and the camera is a high resolution (2048×2048) CCD camera. The field of view (FOV) size is chosen by 150% of the chord length to observe the dynamic stall phenomenon.

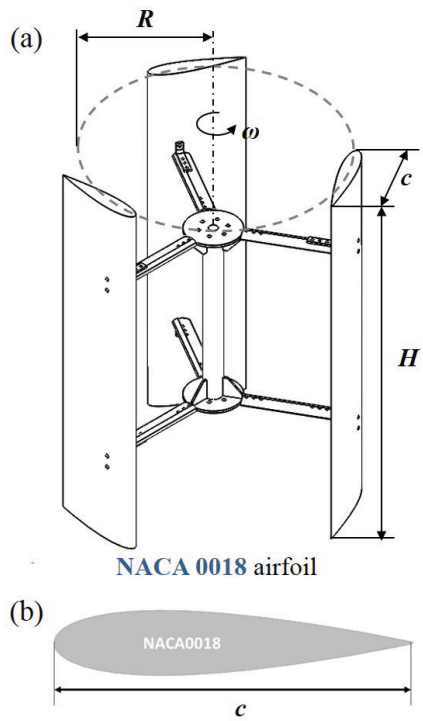

(c)

Blade cross-section	NACA0018
Rotating radius, ***R***	150 mm
Blade height, ***H***	400 mm
Chord, ***c***	90 mm
Number of blades, ***N***	3

Figure 2.1. (a) geometry of VAWT model; (b) a cross section of the NACA0018 airfoil; (c) specification of VAWT model.

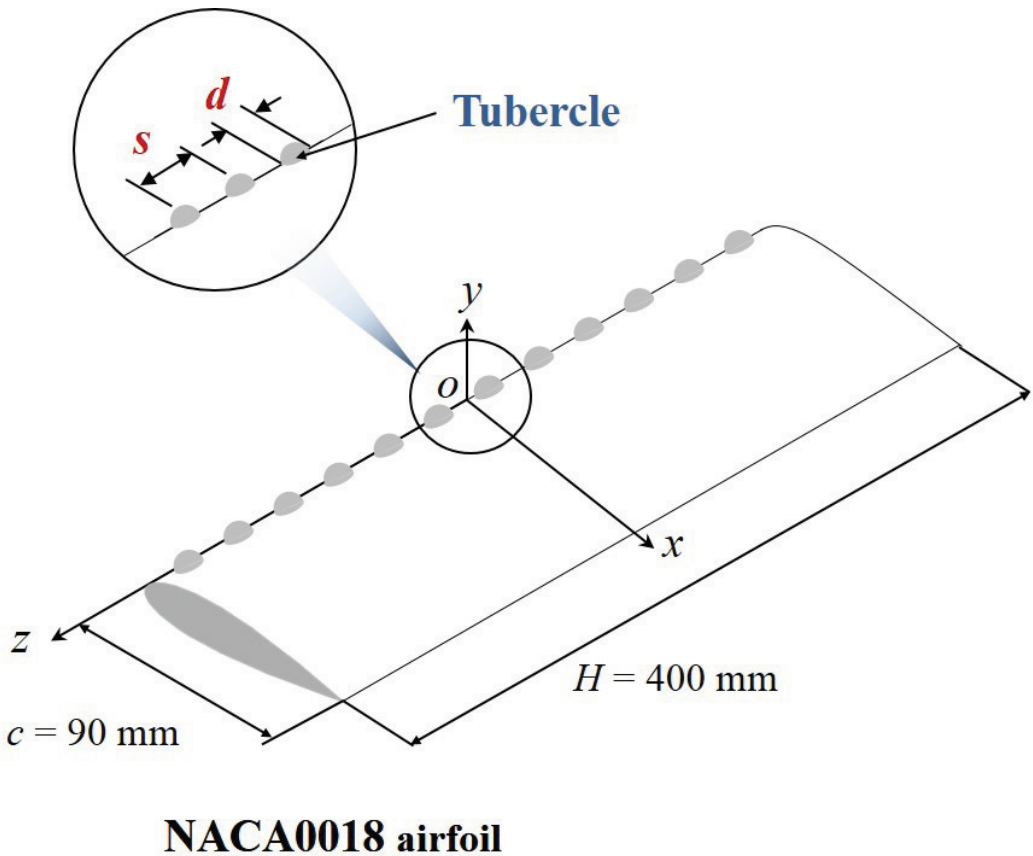

Figure 2.2. Parameters for tubercles.

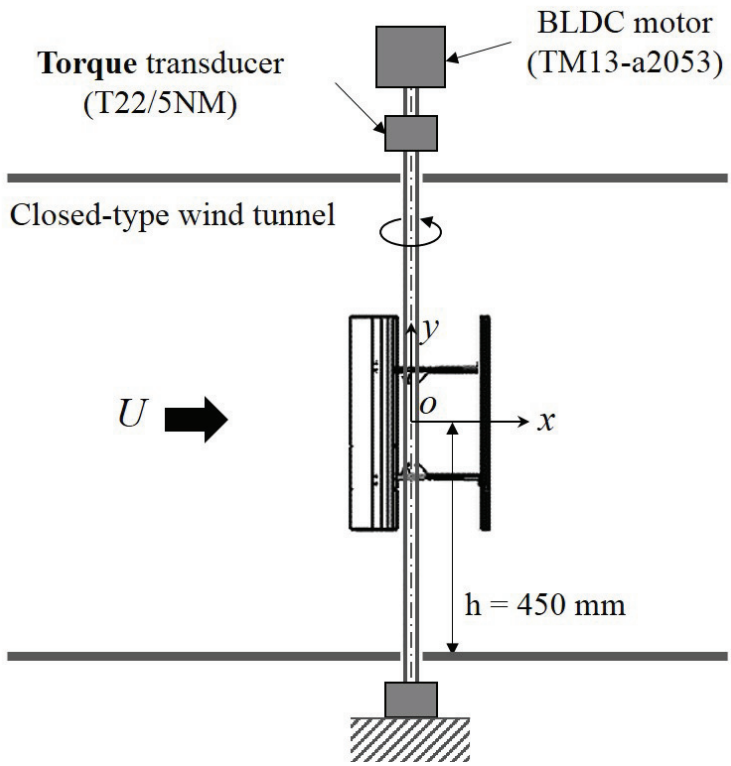

Figure 2.3. Schematic diagram of the torque measurement.

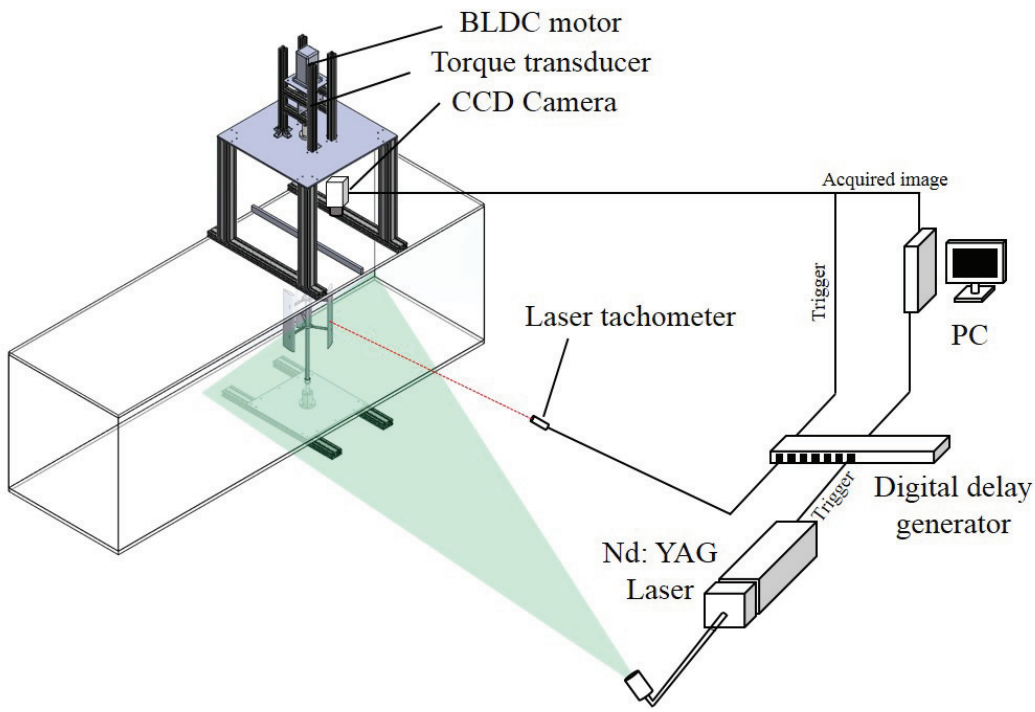

Figure 2.4. Schematic diagram of the PIV measurement.

Chapter 3

Flow Characteristics

3.1 Aerodynamic performance of VAWT

Figure 3.1 shows the measurements of the average power coefficient, C_P , as the tip-speed-ratio was varied. This power coefficient is a measure of the relative kinetic energy extracted from the flow. The average power coefficient is defined as $\bar{C_P} = \bar{P}/(0.5\rho U^3 A)$. ρ is the air density, U is the free stream flow speed and A is the characteristic area, i.e., projected swept area of the rotor. The average power was estimated from the torque measurements as $\bar{P} = \bar{T\omega}$, where T and ω are the instantaneous torque and angular velocity, respectively. The trends in the measured power curves for the turbines are consistent with experimental predictions by Araya et al (2017) for a 3 straight-bladed VAWT. Reynolds number based on rotor diameter of previous research and present study are 0.8×10^5 and 1.2×10^5, respectively. Since Bachant and Wosnik (2014) found that turbine performance becomes nearly independent of Reynolds number above turbine diameter Reynolds number of $Re_D = O(10^5)$, the measured data could be reliable. The difference between them would be any additional applied load, such as bearing friction, an unpowered DC motor and so on. For $C_P > 0$, energy is extracted from the flow on average, as in the case of an operational VAWT. However, for $C_P < 0$, energy is added to flow on average. So, this model turbine operate when $\lambda < 1.5$, otherwise, it

works to the flow. In present study, the model has a maximum value of 1.43 for C_P at $\lambda = 1.05$, and C_p becomes 0 when λ is about 1.8. In other words, if λ is less than 1.8, the VAWT model can generate the power on average, i.e. energy is extracted from the flow on averaged, and if λ is greater than 1.8, the VAWT model cannot generate the power on average, i.e. it work on the flow on average. And the VAWT model produce the biggest energy at $\lambda = 1.05$, which is called λ_{opt}.

3.2 PIV measurements

Figure 3.2 and 3.3 show the mean velocity fields with vorticity contours along the variations of azimuthal angles (θ=60°, 70°, 80°, 90° and 120°) at λ=1.05. The vorticities ω_y have been normalized by the free stream speed U and rotor diameter D. As shown in the Figure 3.2(a), the flow follows along the blade surface of the leading edge, and then the flow shed at the trailing edge when θ=60°. When θ=70°, the flow follows along the blade surface of the leading edge and shed at the trailing edge as similar as flow motion at θ=60° (Figure 3.2(b)). However, the strong counterclockwise vorticity can be observed on the suction surface at the leading edge of the blade. When θ=80°, as it can be seen at Figure 3.2(c), the flow separates and undergoes leading edge vortex formation at suction surface of the blade, and indicate stronger counterclockwise vorticity than that of θ=70°. Then when θ=90°, the flow undergoes dynamic stall at the suction surface of the blade, and fully separating, which result in the strongest counterclockwise vorticity in the measured fields (Figure 3.3(a)). When θ reaches 120°, the dynamic stall vortex finally falls off the blade as it can be seen in Figure 3.3(b). This unsteady separation is assumed to be one of the aerodynamic loss of the VAWT.

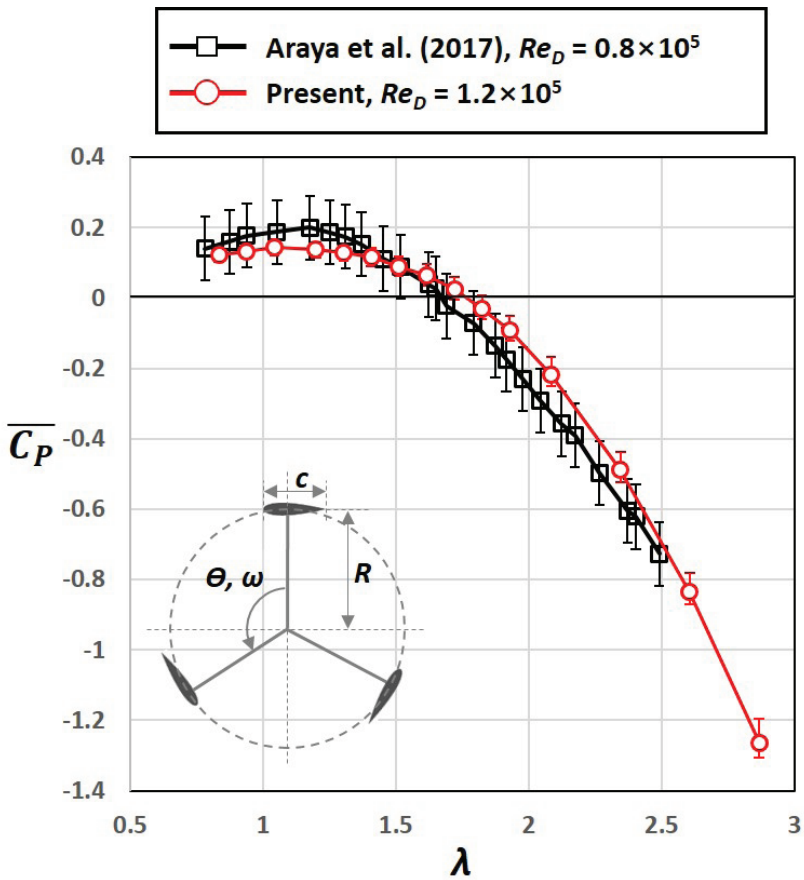

Figure 3.1. Results of torque measurements of VAWT model without tubercles.

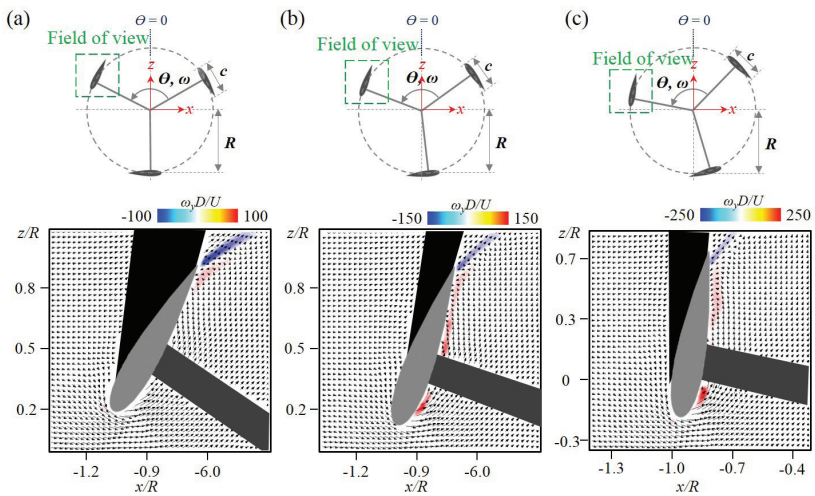

Figure 3.2. Mean velocity fields with vorticity contour: (a) at θ=60° (b) at θ=70° (c) at θ=80°.

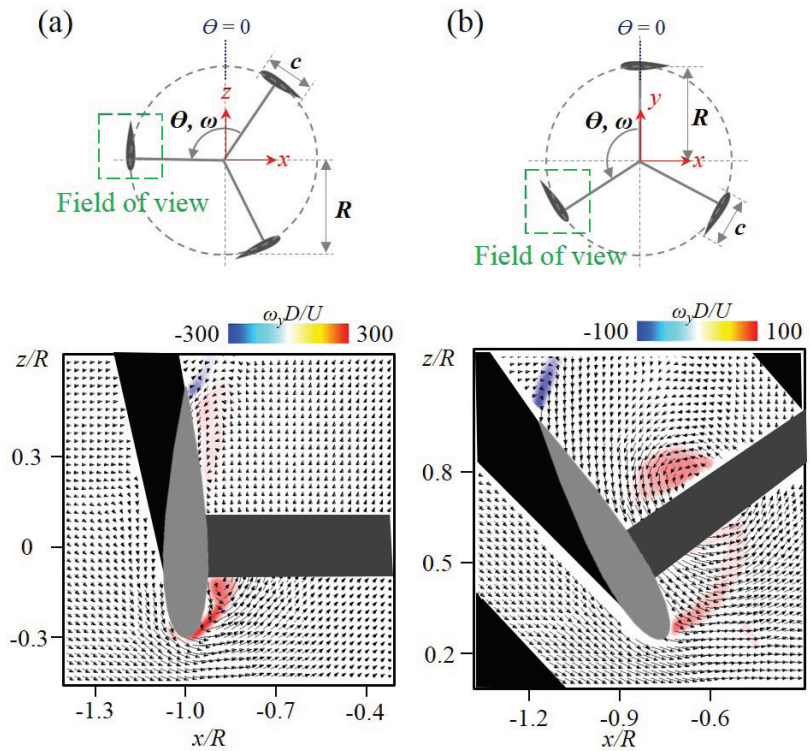

Figure 3.3. Mean velocity fields with vorticity contour: (a) at θ=90° (b) at θ=120°.

Chapter 4

Flow Control

4.1 Control ideas

To control the unsteady flows discussed in Ch. 3, we introduced the leading edge tubercles. As depicted in Ch. 2.2, two parameters are chosen to increase aerodynamic performance by controlling the dynamic stall. Since the full scale of tubercles of the Humpback whales are investigated by previous researchers (Johari *et al.*, 2007; Fish *et al.*, 2011), the domain of diameter (d) of tubercles are 3 mm ($d/c = 0.035$) to 7 mm ($d/c = 0.075$) as increment of 2 mm and the domain of spacing (s) between tubercles are 10 mm ($s/H = 0.025$), 20 mm ($s/H = 0.05$) and 40 mm ($S/H = 0.1$).

4.2 Aerodynamic performance of VAWT with tubercles

Figure 4.1 shows the measurements of the average power coefficient, C_P , on the VAWT model with and without tubercles as the tip-speed-ratio was varied. The average power coefficient of the VAWT model without tubercles are plotted as black diamond symbols. The change of diameter (d) of tubercles is represented by the change of the symbol: the circle symbol is d=5 mm, the triangle symbol is $d = 3$ mm and the square symbol is $d = 7$ mm. The change of spacing (s) between the tubercles is represented by the change of color: the red line is $s = 10$ mm, the blue line is $s = 20$ mm, and the purple

line is $s = 40$ mm. The parameters were tested, and we got the enhancement of aerodynamic performance when $d = 5$ mm and $s = 20$ mm. The aerodynamic performance, indicated as average power coefficient C_P, is improved across the all TSR, especially in λ_{opt} with about 30% efficiency

4.3 PIV measurements

Figure 4.2 to 4.6 show the mean velocity fields with vorticity contours of VAWT model with and without tubercles along the variations of azimuthal angles (θ = 60°, 70°, 80°, 90° and 120°) at λ=1.05. For the VAWT model with tubercles, two types of PIV measurements are conducted to investigate the effect of the tubercles: flow field above the tubercles and flow field between the tubercles. The vorticities ω_y have been normalized by the free stream speed U and rotor diameter D. When the θ=60°, flow field characteristics are similar regardless of tubercles as shown in the Figure 4.2. Flow follows along the blade suction surface of the leading edge, and they shed at the trailing edge. When θ=70°, the flow characteristics are similar as flow motion of before. The flow follows along the blade surface of the leading edge and shed at the trailing edge. There are strong counterclockwise vorticity can be observed regardless of tubercles, but the strength of VAWT models with tubercles are smaller than that without tubercles (Figure 4.3). When θ=80°, there are difference between the VAWT model with and without tubercles. As it can be seen at Figure 4.4, in the VAWT model without tubercles, the flow separates and undergoes dynamic stall leading edge vortex formation on the suction surface of the blade, which indicates stronger counterclockwise vorticity than that of θ=70°. The flow characteristics of VAWT model with tubercles, however, have the difference from that without tubercles. Above the tubercle, there appears to be stronger coun-

terclockwise vorticity than that without tubercles, but there is little vorticity between the tubercles when compared to the other two. Unlike the other two cases (without tubercles and above the tubercles) where the flow separates at the leading edge, the flow between the tubercles follows along the blade surface of leading edge. When θ=90°, the flow undergoes dynamic stall at the suction surface of the blade, and fully separating, which result in the strongest counter-clockwise vorticity in the measured fields regardless of tubercles (Figure 4.5). But strength of vorticity is differ each other: the vorticity between the tubercles are much smaller than the vorticity above the tubercles and the vorticity without tubercles. When θ reaches 120°, the leading edge vortex finally falls off the blades as it can be seen in Figure 4.6.

To investigate the effect of the tubercles, x'-y' plane PIV measurement is conducted at θ=80 where the biggest difference are showed. Streamwise location of $z/c = 0.3$ is chosen. Figure 4.7 shows the mean streamwise vorticity contour with velocity contours. On the blade with tubercles, a counter rotating vortex pair is observed between two tubercles while no significant characteristic is observed on the blade without tubercles. Tubercles acts as a sort of bump to generate streamwise vortices. Byun *et al.* (2004) showed that the bump generate downwash motions induced by streamwise vortices. In other words, tubercles generate streamwise vortices inducing downwash motions, which is delaying flow separation.

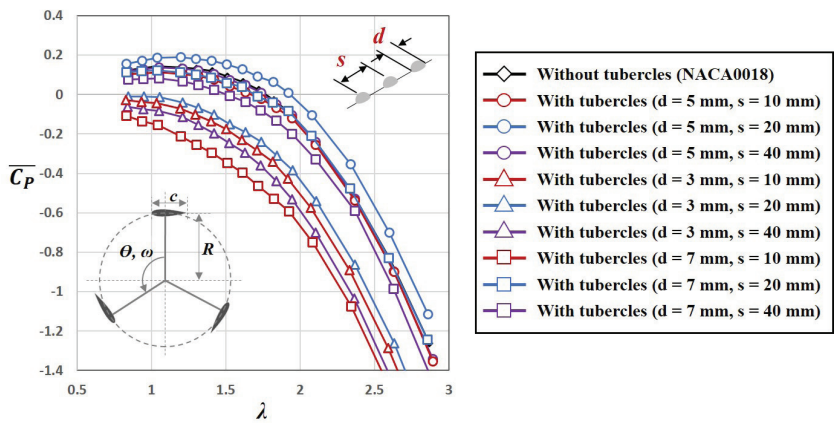

Figure 4.1. Effects of the tubercles on aerodynamic performance of VAWT.

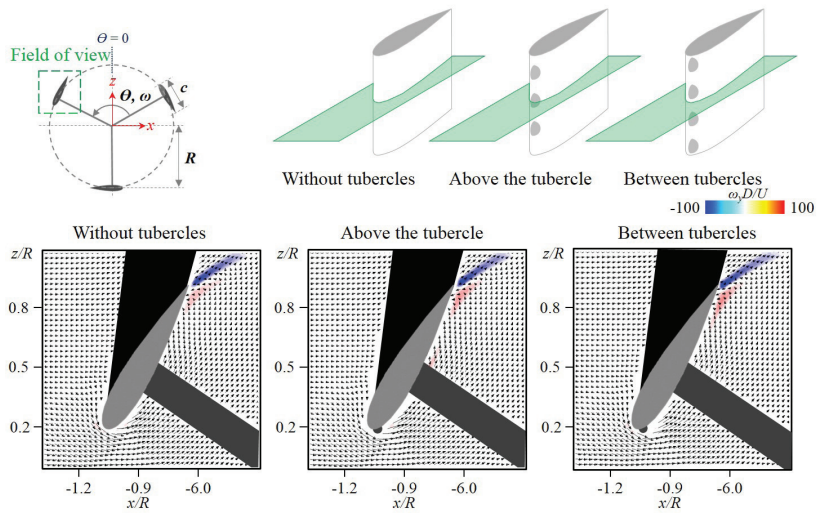

Figure 4.2. Mean velocity fields with vorticity contour of VAWT models with and without tubercles at θ=60°.

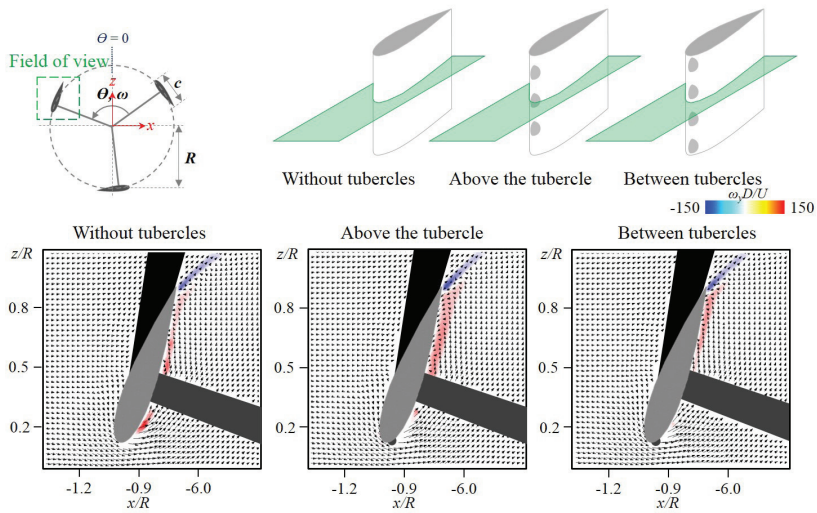

Figure 4.3. Mean velocity fields with vorticity contour of VAWT models with and without tubercles at θ=70°.

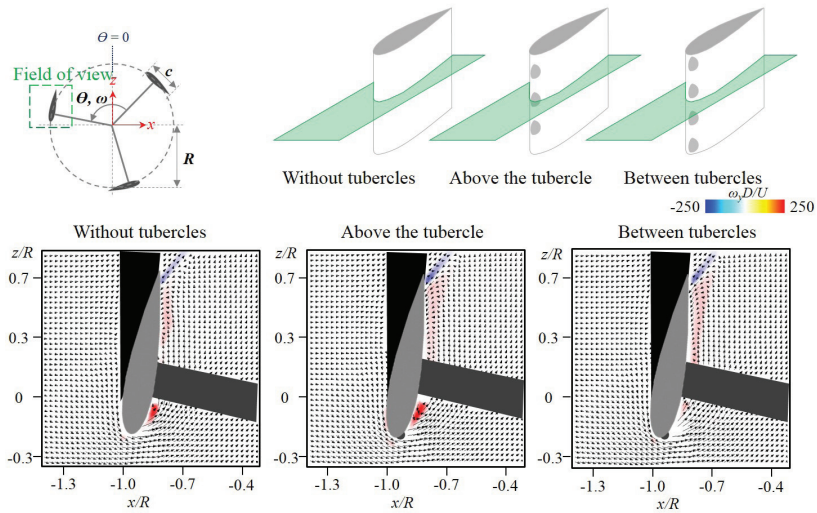

Figure 4.4. Mean velocity fields with vorticity contour of VAWT models with and without tubercles at θ=80°.

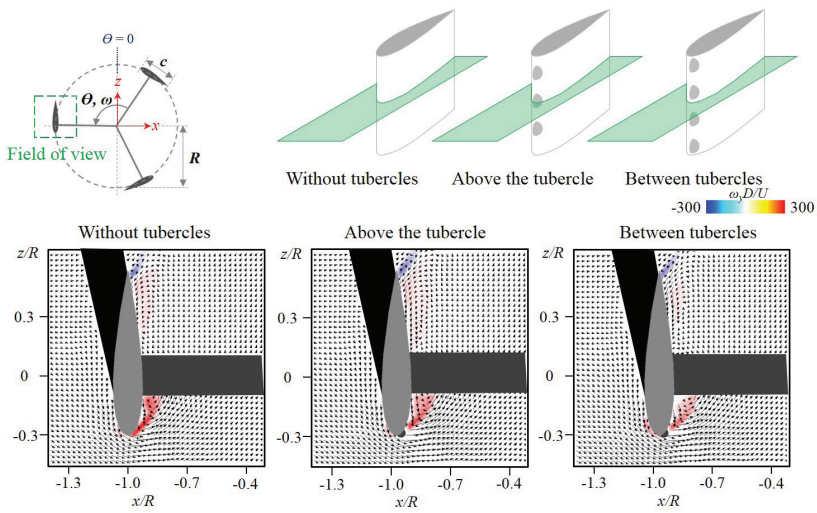

Figure 4.5. Mean velocity fields with vorticity contour of VAWT models with and without tubercles at θ=90°.

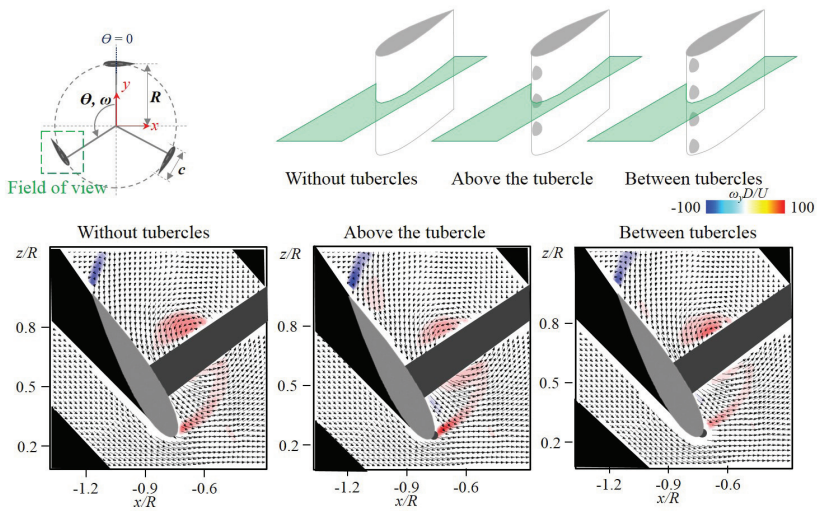

Figure 4.6. Mean velocity fields with vorticity contour of VAWT models with and without tubercles at θ=120°.

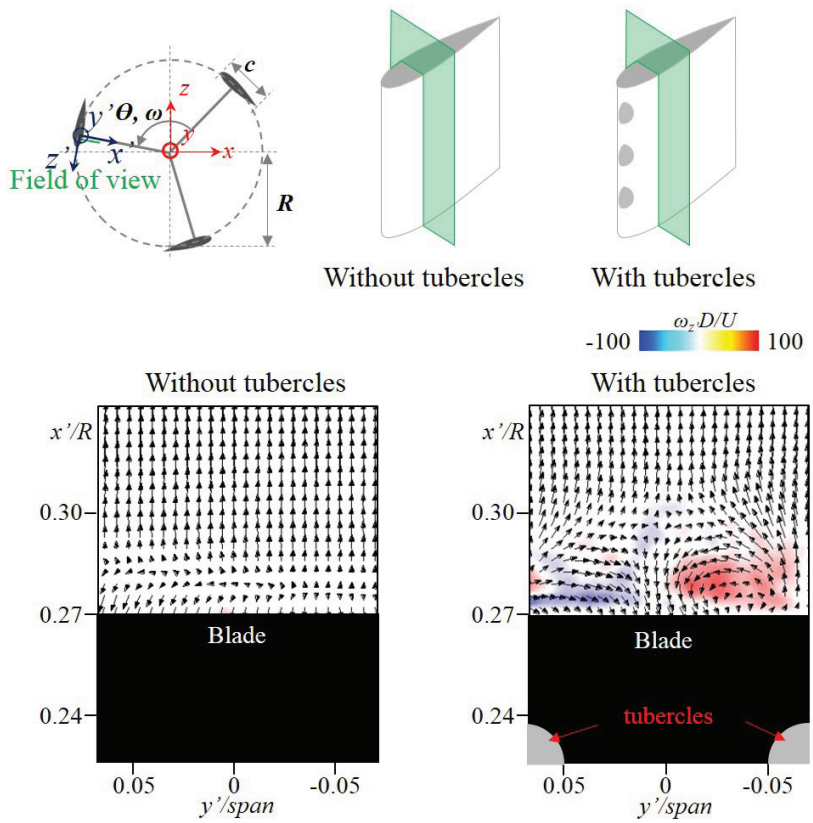

Figure 4.7. Mean velocity fields with vorticity contour of VAWT models with and without tubercles at $x' - y'$ plane.

Chapter 5

Summary and Conclusions

In the present study, we investigated the unsteady flow characteristics of the flow around the vertical axis wind turbine to develop flow control ideas for improving an aerodynamic performance of VAWT. The unsteady flows observed in the VAWT are unsteady separation at blade leading dedge and vortex shedding at blade trailing edge. Especially the dynamic stall phenomenon, resulting in a performance decreases, is observed. Modifying the leading edge by applying the tubercles successfully controlled the unsteady separation for the blade leading edge. The tubercles generated streamwise vortices delaying the flow separation, resulting in a performance enhancement.

References

Araya, D. B. & Dabiri, J. O. 2015 A comparison of wake measurements in motor-driven and flow-driven turbine experiments. *Exp. Fluids* **56**, 1–15.

Araya, D. B., Colonius, T. & Dabiri, J. O. 2017 Transition to bluff-body dynamics in the wake of vertical-axis wind turbines. *J. Fluid Mech.* **813**, 346–381.

Bachant, P. & Wosnik, M. 2015 Characterising the near-wake of a cross-flow turbine. *J. Turbul.* **16**, 971–980.

Dabiri, J. O. 2011 Potential order-of-magnitude enhancement of wind farm power density via counter-rotating vertical-axis wind turbine arrays. *J. Renew. Sustain. Energy* **3**.

Edwards, J. M., Danao, L. A. & Howell, R. J. 2015 PIV measurements and CFD simulation of the performance and flow physics and of a small-scale vertical axis wind turbine. *Wind Energy* **18**, 201–217.

Ferreira, C. S., Van Kuik, G., Van Bussel, G. & Scarano, F. 2009 Visualization by PIV of dynamic stall on a vertical axis wind turbine. *Exp. Fluids* **46**, 97–108.

Fujisawa, N. & Shibuya, S. 2001 Observations of dynamic stall on Darrieus wind turbine blades. *J. Wind Engng Ind. Aerodyn.* **89**, 201–214.

Greenblatt, D., Harav, A. B., & Mueller-Vahl, H. 2013 Mechanism of Dynamic Stall Control on a Vertical Axis Wind Turbine. AIAA Paper No. 2013-0851.

Hau, E. 2013 Wind Turbines: Fundamentals, Technologies, Application, Economics. Springer. viii.

Islam, M., Ting, D. S.-K., & Fartaj, A. 2007 Desirable airfoil features for smaller-capacity straight-bladed VAWT. *Wind Eng.* **31**, 165–196.

Miklosovic, D. S., Murray, M., Howle, L. E., & Fish, F. E. 2004 Leading-edge tubercles delay stall on humpback whale (*Megaptera novaeangliae*) flippers. *Phys. Fluids* **16**, 39–42.

Posa, A., Parker, C. M., Leftwich, M. C., & Balaras, E. 2016 Wake structure of a single vertical axis wind turbine. *Int. J. Heat Fluid Flow*, 1–10.

Tsai, H. C. & Colonius T. 2016 Coriolis effect on dynamic stall in a vertical axis wind turbine. *AIAA Journal* **54**, 216–226.

Vanek, F. & Albright, L. 2008 Energy systems engineering: Evaluation and implementation. McGraw-Hill Education.

Whittlesey, R. W., Liska, S., & Dabiri, J. O. 2008 Fish schooling as a basis for vertical axis wind turbine farm design.. *Bioinspir. Biomim.* **5**.

Fish, F. E., Weber, P. W., Murray, M. M., & Howle L. E. 2011 The tubercles on humpback whales' flippers: application of bio-inspired technology. *IIntegr. Comp. Biol.* **51**, 203–213.

Johari, H., Henoch, C., & Custodio, D., & Levshin, A. 2007 Effects of leading-edge protuberances on airfoil performance. *AIAA journal* **45**, 2634–2642.

Byun, G., Simpson, R. L., & Long, C. H. 2004 Study of vortical separation from three-dimensional symmetric bumps. *AIAA journal* **42**, 754–765.

Narayanan, S., Chaitanya, P., Haeri, S., Joseph, P., Kim, J. W., & Polacsek, C. 2015 Airfoil noise reductions through leading edge serrations. *Phys. Fluids* **27**, 025109.

Kim, H., Kim, J., & Choi, H. 2018 Flow structure modifications by leading-edge tubercles on a 3D wing.. *Bioinspir. Biomim.* **13**.

Howell, R., Qin, N., Edwards, J., & Durrani, N. 2010 Wind tunnel and numerical study of a small vertical axis wind turbine.. *Renew. Energy* **35**, 412-422.

Leishman, JG. 2002 Challenges in modelling the unsteady aerodynamics of wind turbines.. *Wind Energy* **5**, 85-132.

Roh, S. & Kang, S. 2013 Effects of a blade profile, the Reynolds number, and the solidity on the performance of a straight bladed vertical axis wind turbine. *J. Mech. Sci. Technol.* **27**, 3299–3307.

Elkhoury, M., Kiwata, T., & Aoun, E. 2015 Experimental and numerical investigation of a three-dimensional vertical-axis wind turbine with variable-pitch. *J. Wind Eng. Ind. Aerodyn.* **139**, 111–123.

수직축 풍력발전기 주위 유동에 대한 실험적 연구 및 돌기를 이용한 유동 제어

서울대학교 대학원
기계항공공학부
김종현

요 약

본 연구에서는 수직축 풍력발전기 주위 유동의 비정상 유동 특성을 알아보고, 이를 제어함으로써 수직축 풍력발전기의 공력성능을 높이고자 실험적 연구를 수행하였다. 실험은 주 유동 속도와 회전 직경에 기초한 레이놀즈 수 120,000에서 수행하였으며, 운전 조건인 300 - 1100 rpm에서 수행하였다. 수직축 풍력발전기의 성능 계수는 회전식 토크 변환기를 통해 측정하여 주속비에 따른 수직축 풍력발전기의 성능계수 변화를 검증하였으며, 위상평균 영상입자유속계 (Phase-averaged PIV)를 이용하여 속도장을 측정하였다. 발전기가 회전함에 따라 날개의 받음각이 증가하여 날개 주변에서 유동박리와 와류가 발생하고, 날개 전단 흡입면에서 동적 실속이 발생하는 것을 확인하였다. 동적 실속을 제어함으로써 회전익의 공력 성능을 향상시키기 위해 날개 전단 흡입면에 돌기 형상의 유동제어장치를 적용하였다. 그 결과 돌기 형상의 유동제어장치가 유속 방향 와류가 하강운동을 유도하여 동적 실속 발생을 지연시킴으로써, 회전익의 공력 성능을 향상시킬 수 있음을 보였다.

주요어 : 수직축 풍력발전기, 동적 실속, 생체모방 유동제어, 돌기, 유선 방향 와류, 실속 지연
학번 : 2016-20649